Homogenization models for thin rigid structured surfaces and films

Jean-Jacques Marigo, Agnès Maurel

Homogenization models for thin rigid structured surfaces and films

Jean-Jacques Marigo and Agnès Maurel

Laboratoire de Mécanique du Solide, CNRS,

Ecole Polytechnique, Palaiseau, France

Institut Langevin, CNRS, ESPCI ParisTech, Paris, France

Abstract

A homogenization method for thin microstructured surfaces and films is presented. In both cases, sound hard materials are considered, associated with Neumann boundary conditions and the wave equation in the time domain is examined. For a structured surface, a boundary condition is obtained on an equivalent flat wall, which links the acoustic velocity to its normal and tangential derivatives (of the Myers type). For a structured film, jump conditions are obtained for the acoustic pressure and the normal velocity across an equivalent interface (of the Ventcels type). This interface homogenization is based on a matched asymptotic expansion technique, and differs slightly from the classical homogenization, which is known to fail for small structuration thicknesses. In order to get insight into what causes this failure, a two-step homogenization is proposed, mixing classical homogenization and matched asymptotic expansion. Results of the two homogenizations are analyzed in light of the associated elementary problems, which correspond to problems of fluid mechanics, namely, potential flows around rigid obstacles.

I. INTRODUCTION

Acoustic metamaterials consisting in massive materials perforated by periodic subwavelength holes [1–3] or more sparse structures involving a periodic arrangement of wires [4] are able to control the wave propagation with high flexibility. In comparison, phononic crystals have *a priori* higher dimensions because of their wavelength-scale period. However, if the metamaterials have a subwavelength period, many of the observed phenomena are attributable to Fabry-Perot type resonances, resonances in the hole or resonances of the wires. Therefore, these structures have a limitation in their thickness, which has to be at wavelength scale to produce such resonances (and the thickness refers to the size in the direction perpendicular to the planes containing the periodic cells). In order to reduce the size of the devices, structures with a subwavelength thickness have been developed. They are known as metasurfaces and metafilms. Despite the vanishing thickness in comparison to the incident wavelength, the capability of these ultra-thin devices to control the wave propagation has been evidenced. This may be due to resonances which are not trivially related to their thickness. It can be a thin elastic membrane within the unit cell [5, 6], or resonances of labyrinthine or curled elements squeezed in the unit cell [7–9].

Because of their subwavelength periodicity, homogenization techniques are natural tools to describe the effective properties of metamaterials. The classical homogenization has been used successfully to describe the acoustic propagation in thick metamaterial slabs; in this case, an equivalent slab is found, with the same thickness than the original one, and composed of an homogeneous and anisotropic medium with effective bulk modulus and mass density [10, 11]. When metafilms or metasurfaces are concerned, first attempts have been proposed using the same effective parameters as for thick slabs but attributing an *ad hoc* small thickness (see *e.g.* the discussions § 3 in [12] and §2 in [13]). It is now admitted that these approaches are not pertinent and rather, jumps or transition conditions for the fields across an equivalent surface are thought. To that aim, interface homogenizations based on matched asymptotic expansion techniques have been used in different contexts of waves [14–18]. In [19], we presented such interface homogenization following the approach developed in solid mechanics [20, 21]; we considered scalar waves propagating through structured rigid films in the frequency domain and the failure in the classical homogenization was illustrated for thicknesses of the film passing below the inverse of the wavenumber.

The present paper extends this study in the two following senses. First, the problem is considered in the time domain, and the case of structured surfaces is included (the two considered geometries are shown in Fig. 1). The difficulty in considering the equations in the time domain is rather incremental but it allows us to question the equation of energy conservation, and this is not incidental. If we have numerical implementations in mind, for the boundary conditions at an equivalent wall (Fig. 1(a)) or for the jump conditions at an equivalent interface (Fig. 1(b)), these surfaces must be associated to positive energies. This is ensured following the intuitive argument that the numerical domain has to be a truncation of the original domain, where the microstructure has been removed. This is in fact classical in the literature considering thin homogeneous layers [22, 23] but it has been less regarded for thin structured layers (an exception can be found in [18] where the authors refer to non-centered jump conditions). Next, we address the validity of the classical homogenization in a different way than the brut comparison of results coming from a particular scattering problem, as proposed in [19]. In classical homogenization, the bulk of the structured material is replaced by an equivalent homogeneous anisotropic material; a layer of this equivalent material continues to mimic the response of the real structure (and this is a good news, otherwise, classical homogenization would be completely useless). The corresponding layer being homogeneous, one can apply a matched asymptotic expansion technique to determine the effective conditions on a wall or across an interface for vanishing layer thicknesses. This is very similar to the two-step homogenization proposed in [24], but in the present case, we know that the obtained conditions will be unsatisfactory. Nevertheless, it is enlightening to analyze what causes the failure of this (in some sense dishonest) homogenization, and we say that it fails when it differs from the interface homogenization. This is done by analyzing the associated elementary problems, which question flows of perfect fluids around rigid obstacles.

We start with the linearized Euler equations for the acoustic pressure $P(\mathbf{X}, t)$ and velocity $\boldsymbol{U}(\mathbf{X}, t)$, written in the time domain, with t the time and $\mathbf{X} = (X_1, X_2)$ the spatial coordinates

$$\begin{cases} \rho_0 \dfrac{\partial \boldsymbol{U}}{\partial t} = -\boldsymbol{\nabla} P, \\ \chi_0 \dfrac{\partial P}{\partial t} + \mathrm{div} \boldsymbol{U} = 0. \end{cases} \tag{1}$$

In Eqs. (1), ρ_0 is the mass density and $\chi_0 = (\rho_0 c_0^2)^{-1}$ the isentropic compressibility of the

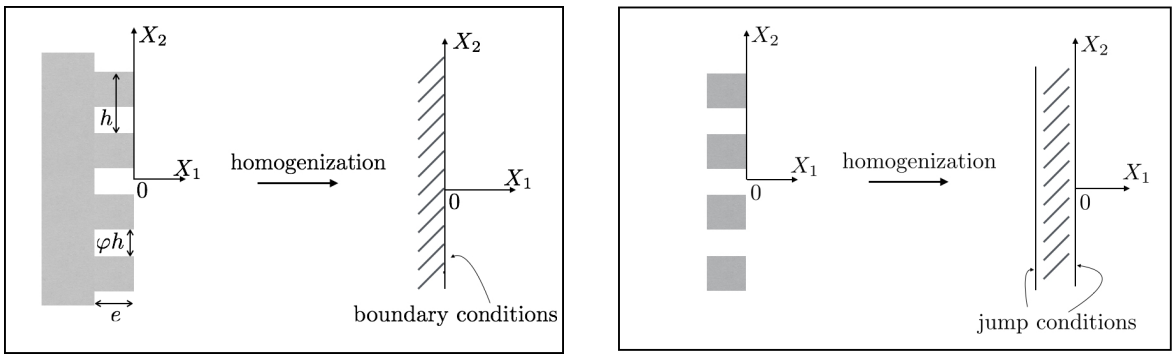

(a) (b)

FIG. 1. (a) Wall structured with periodic rigid roughnesses; the homogenization process gives an equivalent flat wall associated to a boundary condition of the Myers type, Eq. (19), (b) Array of periodic rigid inclusions; the homogenization process gives an equivalent thin interface associated to jump conditions of the Ventcels type, Eqs. (27).

fluid (c_0 denotes the sound speed in the fluid). In a bounded domain Ω, energy conservation reads

$$\frac{d}{dt}\mathcal{E} + \int_{\partial\Omega} dS\ \mathbf{\Pi}.\mathbf{n} = 0,$$

with $\mathcal{E}$ the acoustic energy and $\mathbf{\Pi}$ the Poynting vector

$$\mathcal{E} = \int_{\Omega} dV\ \left[\frac{\rho_0}{2}U^2 + \frac{\chi_0}{2}P^2\right], \quad \mathbf{\Pi} = P\boldsymbol{U}.$$

In the time domain, we consider acoustic waves with a minimum wavelength $2\pi/k$ larger than the typical periodicity of the microstructuration h, such that

$$\varepsilon \equiv kh \ll 1.$$

To be consistent, we will work in dimensionless coordinates. We define

$$\mathbf{x} \equiv k\mathbf{X}, \quad \tau \equiv kc_0 t,$$

and

$$\boldsymbol{u}(\mathbf{x},\tau) \equiv \rho_0 c_0 \boldsymbol{U}(\mathbf{X},t), \quad p(\mathbf{x},\tau) \equiv P(\mathbf{X},t).$$

Now, the Eqs. (1) read in dimensionless form

$$\begin{cases} \dfrac{\partial \boldsymbol{u}}{\partial \tau} = -\boldsymbol{\nabla}_{\mathbf{x}} p, \\ \dfrac{\partial p}{\partial \tau} + \mathrm{div}_{\mathbf{x}}\boldsymbol{u} = 0. \end{cases} \tag{2}$$

In principle, the presented homogenizations apply in three dimensions, and for any shape of structurations, including 3D structurations. In order to get explicit conditions, we shall restrict ourselves to the case of two dimensional layered structurations; we shall specify when the calculations loose in generality.

II. HOMOGENIZATION OF MICRO-STRUCTURED SURFACES

We consider a rigid wall with periodic roughnesses, Fig. 1(a) (to anticipate, a layered structuration is shown, but as previously said, more involved structurations in two and three dimensions can be considered).

A. The matched asymptotic expansion

1. Inner and outer expansions

The idea is to expand the solutions of Eqs. (2) with respect to the small parameter ε, namely

$$\begin{cases} p = p^0(\mathbf{x},\tau) + \varepsilon p^1(\mathbf{x},\tau) + \varepsilon^2 p^2(\mathbf{x},\tau) + \dots, \\ \\ \boldsymbol{u} = \boldsymbol{u}^0(\mathbf{x},\tau) + \varepsilon \boldsymbol{u}^1(\mathbf{x},\tau) + \varepsilon^2 \boldsymbol{u}^2(\mathbf{x},\tau) + \dots. \end{cases} \tag{3}$$

In principle, this expansion can be used in the whole space (see *e.g.* [14]). Nevertheless, if the spatial derivatives in Eq. (2) make ε to appear, the resolution may become tricky. Such complications are avoided if a displacement in $\mathbf{x}$ of order unity produces a variation in p and $\boldsymbol{u}$ of order unity, namely $\partial_{x_i} p \sim p$. This is ensured in the far field, that is far enough from the wall, where $\partial_{X_i} P \sim kP \to \partial_{x_i} p \sim p$. The story is different in the near field: there, the roughnesses generate evanescent waves whose strongest variations are associated to the smallest scales of the microstructure, say $\partial_{X_i} P \sim P/h \to \partial_{x_i} p \sim p/\varepsilon$. The wavefield has also variations when moving along the interface which are associated to the typical central wavelength. This behavior is associated to low variations of p (for which $\partial_{x_2} p \sim p$). Thus, we have to deal with different scales in the far and near fields, and with two scales in the near field.

The presented approach uses two ingredients to account for these multiple scales: first, a

separation of the space into an inner and an outer regions, which correspond to the near and far fields, respectively. In the outer region, the natural coordinate $\mathbf{x} \equiv (x_1, x_2)$ is adapted and the expansions in Eq. (3) applies. In the inner region, a new system of coordinates $\mathbf{y} = \mathbf{x}/\varepsilon$ is used which accounts for the rapid variations of the evanescent fields ($\partial_{y_i} p \sim p$). Next, the slow variations along x_2 are accounted for by keeping x_2 as additional coordinate. Owing to these modifications, the expansions read

$$\text{Outer exp.} \begin{cases} p = p^0(\mathbf{x}, \tau) + \varepsilon p^1(\mathbf{x}, \tau) + \dots, \\ \\ \boldsymbol{u} = \boldsymbol{u}^0(\mathbf{x}, \tau) + \varepsilon \boldsymbol{u}^1(\mathbf{x}, \tau) + \dots \end{cases} \tag{4}$$

$$\text{Inner exp.} \begin{cases} p = q^0(\mathbf{y}, x_2, \tau) + \varepsilon q^1(\mathbf{y}, x_2, \tau) + \dots, \\ \\ \boldsymbol{u} = \boldsymbol{v}^0(\mathbf{y}, x_2, \tau) + \varepsilon \boldsymbol{v}^1(\mathbf{y}, x_2, \tau) + \dots \end{cases}$$

and the terms $(q^n, \boldsymbol{v}^n)$, $n = 0, 1, \dots$, of the inner solution are assumed to be periodic *w.r.t.* y_2. Now, Eqs. (2) can be written in the inner and in the outer regions, owing to the expressions of the differential operator

$$\begin{cases} \boldsymbol{\nabla} \to \boldsymbol{\nabla}_{\mathbf{x}}, & \text{in the outer problem,} \quad \text{(5a)} \\ \boldsymbol{\nabla} \to \dfrac{1}{\varepsilon} \boldsymbol{\nabla}_{\mathbf{y}} + \dfrac{\partial}{\partial x_2} \mathbf{e}_2, & \text{in the inner problem.} \quad \text{(5b)} \end{cases}$$

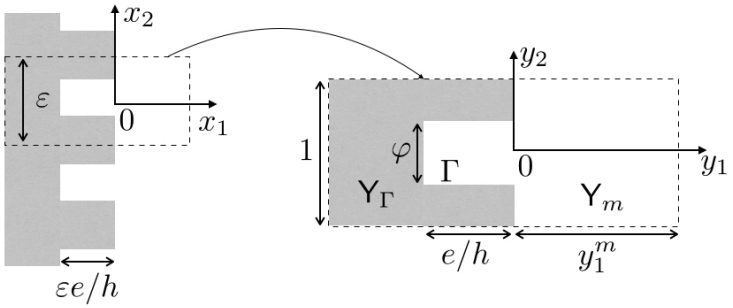

FIG. 2. The wall structured by periodic roughnesses in the two systems of coordinates $\mathbf{x}$ and $\mathbf{y}$. In $\mathbf{y}$-coordinates, Y_Γ and Y_m denote the regions occupied by the rigid material and by the air respectively ($\mathsf{Y} = \lim_{y_1^m \to +\infty} \mathsf{Y}_m$); Γ is the boundary of Y_Γ where Neumann boundary condition applies. $\mathcal{S}_c = e\varphi/h$ is the dimensionless surface of air in the groove.

Thanks to the periodicity of $(q^n, \boldsymbol{v}^n)$ *w.r.t.* y_2, we shall consider the domain $\mathsf{Y}_m^t = (0, y_1^m) \times (-1/2, 1/2)$ in $\mathbf{y}$ coordinate (Fig. 2). Y_Γ is the domain occupied by the rigid

material, and Neumann boundary conditions apply on the boundary Γ of Y_Γ in contact with the air. Next, we define $\mathsf{Y}_m = \mathsf{Y}_m^t \backslash \mathsf{Y}_\Gamma$ and the unit cell corresponds to $\mathsf{Y} = \lim_{y_1^m \to \infty} \mathsf{Y}_m$. Inside Y, the air groove has a thickness e/h along y_1 and a height φ along y_2; we denote $\mathcal{S}_c = e\varphi/h$ the corresponding surface.

Finally, it is worth noting that, in the three dimensional case, it is sufficient to replace x_2 by $\mathbf{x}' = (x_2, x_3)$ and the calculations are the same than in two dimensions.

2. Equations at orders 0 and 1

We start by reporting the equations that will be needed in the following. For the outer solution, using Eq. (5a), Eqs. (2) are at the leading order

$$\begin{cases} \dfrac{\partial \boldsymbol{u}^0}{\partial \tau} = -\boldsymbol{\nabla}_{\mathbf{x}} p^0, & \text{(6a)} \\ \dfrac{\partial p^0}{\partial \tau} + \mathrm{div}_{\mathbf{x}} \boldsymbol{u}^0 = 0, & \text{(6b)} \end{cases}$$

and for the inner solution, using Eq. (5b), we get

$$\begin{cases} \boldsymbol{\nabla}_{\mathbf{y}} q^0 = 0, & \text{(7a)} \\ \mathrm{div}_{\mathbf{y}} \boldsymbol{v}^0 = \mathbf{0}, & \text{(7b)} \\ \dfrac{\partial \boldsymbol{v}^0}{\partial \tau} + \dfrac{\partial q^0}{\partial x_2}\, \mathbf{e}_2 + \boldsymbol{\nabla}_{\mathbf{y}} q^1 = 0, & \text{(7c)} \\ \dfrac{\partial q0}{\partial \tau} + \dfrac{\partial v_2^0}{\partial x_2} + \mathrm{div}_{\mathbf{y}} \boldsymbol{v}^1 = 0. & \text{(7d)} \end{cases}$$

Next, the equations Eqs. (6)-(7) together with the boundary conditions and the matching conditions will be used to find the conditions to be applied on an equivalent surface.

3. Boundary conditions and matching conditions

Because of the separation of the space into two regions, something has to be said on the boundary conditions. By construction, the rigid roughnesses are seen by the inner solution only, and the Neumann boundary condition applies

$$\boldsymbol{v}^n . \mathbf{n}_{|\Gamma} = 0, \ n = 0, 1, \ldots \tag{8}$$

The outer solution does not see the roughnesses (also by construction) but it has to match the inner solution in some intermediate region. These matching conditions will be written following [20] for $x_1 \to 0^+$ corresponding to $y_1 \to +\infty$ (and we denote $f(0)$ the limit value of f for $x_1 \to 0^+$). To do so, we use Taylor expansions of $p^0(x_1, x_2, \tau) = p^0(0, x_2, \tau) + x_1 \partial_{x_1} p^0(0, x_2, \tau) + \cdots = p^0(0, x_2, \tau) + \varepsilon y_1 \partial_{x_1} p^0(0, x_2, \tau) + \ldots$, same for $\boldsymbol{u}^0$. Identifying the terms in ε^n, $n = 0, 1$ in the inner and outer expansions, Eqs. (4), we get, for $n = 0$

$$\begin{cases} p^0(0, x_2, \tau) = \lim\limits_{y_1 \to +\infty} q^0(\mathbf{y}, x_2, \tau), & \text{(9a)} \\ \boldsymbol{u}^0(0, x_2, \tau) = \lim\limits_{y_1 \to +\infty} \boldsymbol{v}^0(\mathbf{y}, x_2, \tau), & \text{(9b)} \end{cases}$$

and for $n = 1$, we shall need only the matching condition for $\boldsymbol{u}^1$

$$\boldsymbol{u}^1(0, x_2, \tau) = \lim_{y_1 \to +\infty} \left[\boldsymbol{v}^1(\mathbf{y}, x_2, \tau) - y_1 \frac{\partial \boldsymbol{u}^0}{\partial x_1}(0, x_2, \tau) \right]. \tag{10}$$

When not needed, the dependance of the functions on the spatial variables and on the time are omitted for readability.

B. Determination of the equivalent boundary condition

1. Solutions at order 0

First, the Eq. (7a) tells us that q^0 does not depend on $\mathbf{y}$, and from the matching condition Eq. (9a), we get

$$q^0(x_2, \tau) = p^0(0, x_2, \tau). \tag{11}$$

Next, integrating the Eq. (7b) over Y gives explicitly the value of $u_1^0(0, x_2, \tau)$, with

$$0 = \int_{\mathsf{Y}} \mathrm{d}\mathbf{y} \ \mathrm{div}_{\mathbf{y}} \boldsymbol{v}^0 = \int_{-1/2}^{1/2} \mathrm{d}y_2 \ v_1^0(+\infty, y_2, x_2, \tau) = u_1^0(0, x_2, t),$$

where we have used the boundary condition, Eq. (8) for $n = 0$, and the matching condition Eq. (9b). The normal acoustic velocity vanishes on the equivalent surface at $x_1 = 0$. This means that the structuration on the wall is not visible at the leading order and the surface behaves as a flat rigid wall; thus, to capture the effect of the structuration, we need to go at order 1, and we are looking for $u_1^1(0, x_2, t)$.

2. Solutions at order 1 and elementary problems

Before going further, we have to define the elementary problem which makes equivalent surface parameters to appear. To that aim, we inspect the Eqs. (7b)-(7c), (8) (for $n = 0$) and (9b), owing to Eq. (11); we get

$$\begin{cases} \Delta_{\mathbf{y}} q^1 = \mathbf{0}, \\ \left[\dfrac{\partial p^0}{\partial x_2}(0, x_2, \tau)\ \mathbf{e}_2 + \boldsymbol{\nabla}_{\mathbf{y}} q^1 \right] . \mathbf{n}_{|\Gamma} = 0, \\ \lim\limits_{y_1 \to +\infty} \boldsymbol{\nabla}_{\mathbf{y}} q^1 = \dfrac{\partial p^0}{\partial x_1}(0, x_2, \tau)\ \mathbf{e}_1. \end{cases} \tag{12}$$

The first and second equations are simply the time derivative versions of Eqs. (7b) and (8), using the Eqs. (7c) and (11) in both cases. The third equation is less immediate although straightforward; consider the time derivative of Eq. (9b), with Eq. (7c)

$$\frac{\partial \boldsymbol{u}^0}{\partial \tau}(0, x_2, \tau) = - \lim_{y_1 \to +\infty} \left[\frac{\partial p^0}{\partial x_2}(0, x_2, \tau)\ \mathbf{e}_2 + \boldsymbol{\nabla}_{\mathbf{y}} q^1 \right],$$

which leads to the desired equation using Eq. (6a). Now, because $u_1^0(0, x_2, \tau) = 0$, its time derivative is zero as well and from Eq. (6a), we have

$$\frac{\partial p^0}{\partial x_1}(0, x_2, \tau) = 0.$$

The system (12) simplifies to

$$\begin{cases} \Delta_{\mathbf{y}} q^1 = \mathbf{0}, \\ \left[\dfrac{\partial p^0}{\partial x_2}(0, x_2, \tau)\ \mathbf{e}_2 + \boldsymbol{\nabla}_{\mathbf{y}} q^1 \right] . \mathbf{n}_{|\Gamma} = 0, \\ \lim\limits_{y_1 \to +\infty} \boldsymbol{\nabla}_{\mathbf{y}} q^1 = \mathbf{0}, \end{cases} \tag{13}$$

being linear with respect to $\partial_{x_2} p^0(0, x_2, \tau)$. Thus, defining $Q^{(2)}$ such as

$$q^1(\mathbf{y}, x_2, \tau) = \frac{\partial p^0}{\partial x_2}(0, x_2, \tau) Q^{(2)}(\mathbf{y}) + Q(\mathbf{x}, \tau), \tag{14}$$

it is sufficient that $Q^{(2)}$ satisfies

$$\begin{cases} \Delta Q^{(2)} = 0, \\ \left[\mathbf{e}_2 + \boldsymbol{\nabla} Q^{(2)} \right] . \mathbf{n}_{|\Gamma} = 0, \\ \lim\limits_{y_1 \to +\infty} \boldsymbol{\nabla} Q^{(2)} = \mathbf{0}, \end{cases} \tag{15}$$

to ensure that q^1 satisfies Eqs. (13). The field $Q^{(2)}$ is an evanescent field being excited at the structured surface (and because $Q^{(2)}$ is defined up to a constant, we can set this constant to 0 without loss of generality). Finally, note that $Q(\mathbf{x},\tau)$ is introduced since the Eqs. (13) define q^1 up to a function independent of $\mathbf{y}$; we will see that the determination of Q is not needed.

3. Boundary condition at the equivalent surface and determination of the surface parameters

To define the boundary condition, we want $u_1^1(0,x_2,\tau)$ (we already know that $u_1^0(0,x_2,\tau)=0$), and $u_1^1(0,x_2,\tau)$ is given by $v_1^1(+\infty,y_2,x_2,\tau)$ in the matching condition, Eq. (10). The limit of v_1^1 will be obtained by integrating the Eq. (7d) over Y. But before, we inspect $\boldsymbol{v}^0$ in Eq. (7c) (because v_2^0 is needed in Eq. (7d)). Using the Eq. (14) in Eq. (7c), we have

$$\frac{\partial \boldsymbol{v}^0}{\partial \tau} = -\frac{\partial p^0}{\partial x_2}(0,x_2,\tau)\left[\mathbf{e}_2+\boldsymbol{\nabla}_{\mathbf{y}}Q^{(2)}\right] = \frac{\partial u_2^0}{\partial \tau}(0,x_2,\tau)\left[\mathbf{e}_2+\boldsymbol{\nabla}_{\mathbf{y}}Q^{(2)}\right], \tag{16}$$

and the latter equality is obtained using the Eq. (6a). Assuming that $\boldsymbol{u}^0=0$ and $\boldsymbol{v}^0=0$ at $\tau=-\infty$ (the acoustic source has been switched on at some initial time), the above identity is valid omitting the time derivative, specifically

$$\boldsymbol{v}^0 = u_2^0(0,x_2,\tau)\left[\mathbf{e}_2+\boldsymbol{\nabla}_{\mathbf{y}}Q^{(2)}\right].$$

We can come back to the Eq. (7d), which is written using Eqs. (11)

$$0=\frac{\partial p_0}{\partial \tau}(0,x_2,\tau)+\frac{\partial u_2^0}{\partial x_2}(0,x_2,\tau)\left[1+\frac{\partial Q^{(2)}}{\partial y_2}\right]+\mathrm{div}_{\mathbf{y}}\boldsymbol{v}^1 = \frac{\partial u_2^0}{\partial x_2}(0,x_2,\tau)\,\frac{\partial Q^{(2)}}{\partial y_2}-\frac{\partial u_1^0}{\partial x_1}(0,x_2,\tau)+\mathrm{div}_{\mathbf{y}}\boldsymbol{v}^1,$$

and the latter equality has been obtained using Eq. (6b). It is now sufficient to integrate the above equation over Y_m to find

$$\frac{\partial u_2^0}{\partial x_2}(0,x_2,\tau)\int_{\mathsf{Y}_m}\mathrm{d}\mathbf{y}\,\frac{\partial Q^{(2)}}{\partial y_2}+\int_{-1/2}^{1/2}\mathrm{d}y_2\left[v_1^1(y_1^m,y_2,x_2,\tau)-(y_1^m+\mathcal{S}_c)\,\frac{\partial u_1^0}{\partial x_1}(0,x_2,\tau)\right]=0. \tag{17}$$

Here, it is important to stress that $(y_1^m+\mathcal{S}_c)$ is the surface of the integration domain Y_m. It is independent on the choice of the origine $y_1=0$, but each term y_1^m and $\mathcal{S}_c$ *does depend on the origine* $y_1=0$. We will come back to this point, which is not incidental,

later. Finally, note that, with our choice of the origine, $\mathcal{S}_c$ is simply the surface of air in the grooves in dimensionless form, and the result holds for any shape of the inclusions (it would be a volume in three dimensions).

Taking the limit $y_1^m \to +\infty$ in (17), and using the matching condition Eq. (10), we finally get

$$u_1^1(0, x_2, \tau) = \mathcal{S}_c \, \frac{\partial u_1^0}{\partial x_1}(0, x_2, \tau) + \mathcal{C} \, \frac{\partial u_2^0}{\partial x_2}(0, x_2, \tau),$$

where we have defined

$$\mathcal{C} \equiv - \int_{\Upsilon} \mathrm{d}\mathbf{y} \, \frac{\partial Q^{(2)}}{\partial y_2}. \tag{18}$$

It is now time to come back to the real space. With $u_1 = u_1^0 + \varepsilon u_1^1 + O(\varepsilon^2)$, we have, up to $O(\varepsilon^2)$

$$u_1(0, x_2, \tau) = \varepsilon \mathcal{S}_c \, \frac{\partial u_1}{\partial x_1}(0, x_2, \tau) + \varepsilon \mathcal{C} \, \frac{\partial u_2}{\partial x_2}(0, x_2, \tau),$$

and finally, introducing φ the filling fraction of air in the groove (whence $\mathcal{S}_c = \varphi e/h$), we get

$$U_1(0, X_2, t) = e\varphi \, \frac{\partial U_1}{\partial X_1}(0, X_2, t) + h\mathcal{C} \, \frac{\partial U_2}{\partial X_2}(0, X_2, t). \tag{19}$$

C. Energy conservation in the homogenized problem

The choice of the origine $y_1 = 0$ has conditioned the parameter $\mathcal{S}_c$ in the Eq. (19). It conditionnes as well the position of the equivalent surface where the boundary condition (19) applies: it is at the edge of the roughnesses. In the homogenized problem, a part of the domain Ω in the original problem has disappeared; let Ω_e being this domain (Fig. 3). In the original problem, the acoustic energy is

$$\mathcal{E} = \int_{\Omega} dV \left[\frac{\rho_0}{2} U^2 + \frac{\chi_0}{2} P^2 \right],$$

and in the homogenized problem, it is

$$\mathcal{E}_h = \int_{\Omega \setminus \Omega_e} dV \left[\frac{\rho_0}{2} U^2 + \frac{\chi_0}{2} P^2 \right] + \mathcal{E}_S,$$

where $\mathcal{E}_S$ is the energy of the equivalent surface, that we expect to account for the acoustic energy in Ω_e, thus that we expect to be positive. Let us inspect the expression of $\mathcal{E}_S$. The

energy conservation in the homogenized problem reads

$$\frac{d}{dt}\int_{\Omega\backslash\Omega_e} dV\ \left[\frac{\rho_0}{2}U^2+\frac{\chi_0}{2}P^2\right]-\int_{X_1=0}\mathrm{d}X_2\ PU_1+\int dS\ \mathbf{\Pi}.\mathbf{n}=0,$$

and from what has been said, $I\equiv-\int_{X_1=0}\mathrm{d}X_2\ PU_1$ has to be the time derivative of a positive quantity. Applying the boundary conditions, Eqs. (19), and using Eqs. (1), we get

$$I=-\int_{X_1=0}\mathrm{d}X_2\left[e\varphi\ P\frac{\partial U_1}{\partial X_1}+h\mathcal{C}\ P\frac{\partial U_2}{\partial X_2}\right],$$

leading to $I=d\mathcal{E}_s/dt$, with

$$\mathcal{E}_s=\int_{X_1=0}\mathrm{d}X_2\left[\frac{\rho_0}{2}(e\varphi-h\mathcal{C})\ U_2^2+\frac{\chi_0}{2}e\varphi\ P^2\right]. \tag{20}$$

Note that the integration by part of $P\partial_{X_2}U_2$ makes the boundary term $[U_2P]_{X_2}$ to appear, and something should be said at both extremities of the equivalent surface; this is disregarded in the present paper. Obviously $e\varphi$ is positive and we will see that $e\varphi-h\mathcal{C}$ is positive as well (see Sec. IV and Appendix A). It follows that the energy associated to the equivalent wall is positive, and the homogenized problem is well suited for numerical purpose.

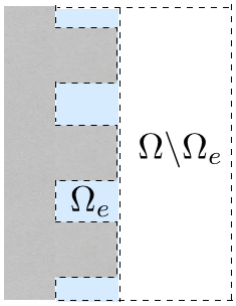

FIG. 3. The domain Ω in the actual problem with the structured wall will be replaced by the domain $\Omega\backslash\Omega_e$ in the homogenized problem.

III. HOMOGENIZATION OF A MICRO-STRUCTURED FILM

For the problem of a micro-structured film (or array), jump conditions are sought, and the jump conditions will be applied to a thin interface of thickness e. To that aim, we define, for any $a>0$

$$[\![f]\!]\equiv f(0^+)-f(-a),\quad \overline{f}\equiv\frac{1}{2}\left[f(0^+)+f(-a)\right].$$

We have two systems of coordinates, $\mathbf{X}$ and $\mathbf{x}$; to avoid heavy notations, we use $[\![f]\!]$ for $a = e$ in $\mathbf{X}$-coordinates and for $a = ke = \varepsilon e/h$ in $\mathbf{x}$-coordinates. We denote in the following

$$\varepsilon' \equiv \varepsilon e/h,$$

and assuming $e/h = O(1)$, $\varepsilon' = O(\varepsilon)$ is a small parameter. Next, following [22, 23], we identify $f(-\varepsilon')$ to $f(0^-)$ and, when $[\![f]\!] = 0$, $f(-\varepsilon') = f(0^+)$ to $f(0)$; in [22], this is done owing to a shift in the $\mathbf{y}$ coordinates to restore the contact, at $y_1 = 0$, between the two faces at $y_1 = -\varepsilon', 0$ of the thin interface, and in [23], this is done introducing generalized jump conditions defined at the mean position between the two faces of the thin interface. Note that an alternative derivation can be performed by 1) defining the jump conditions across a zero thickness interface as done in [19], afterwards jump conditions across an "enlarged" interface are deduced, as in [18]; this is done in the Appendix B.

A. The matched asymptotic expansion

This case is more involved than the previous one but most of the work has been done already. We start with the same ingredients as presented in Sec. II. Only the matching conditions change, being needed at both sides of the equivalent interface of thickness e, and they will be needed at orders 0 and 1 for p and u_1. Next, the Taylor expansions (omitting the variables x_2, τ) read $p^0(x_1 > 0) = p^0(0^+) + \varepsilon y_1 \partial_{x_1} p^0(0^+)$ and $p(x_1 < 0) = p^0(0^-) + \varepsilon(y_1 + e/h)\partial_{x_1} p^0(0^-)$, up to $O(\varepsilon^2)$. It follows that, at order 0 and similarly to Eqs. (9), we have

$$\begin{cases} p^0(0^\pm, x_2, \tau) = \lim\limits_{y_1 \to \pm\infty} q^0(\mathbf{y}, x_2, \tau), & \text{(21a)} \\ \boldsymbol{u}^0(0^\pm, x_2, \tau) = \lim\limits_{y_1 \to \pm\infty} \boldsymbol{v}^0(\mathbf{y}, x_2, \tau), & \text{(21b)} \end{cases}$$

and, at order 1, we have non symmetrical matching conditions, with

$$\begin{cases} p^1(0^-, x_2, \tau) = \lim\limits_{y_1 \to -\infty} \left[q^1(\mathbf{y}, x_2, \tau) - \left(y_1 + \dfrac{e}{h} \right) \dfrac{\partial p^0}{\partial x_1}(0^-, x_2, \tau) \right], & \text{(22a)} \\ \boldsymbol{u}^1(0^-, x_2, \tau) = \lim\limits_{y_1 \to -\infty} \left[\boldsymbol{v}^1(\mathbf{y}, x_2, \tau) - \left(y_1 + \dfrac{e}{h} \right) \dfrac{\partial \boldsymbol{u}^0}{\partial x_1}(0^-, x_2, \tau) \right], & \text{(22b)} \end{cases}$$

and

$$\begin{cases} p^1(0^+, x_2, \tau) = \lim\limits_{y_1 \to +\infty} \left[q^1(\mathbf{y}, x_2, \tau) - y_1 \dfrac{\partial p^0}{\partial x_1}(0^+, x_2, \tau) \right], & \text{(23a)} \\ \boldsymbol{u}^1(0^+, x_2, \tau) = \lim\limits_{y_1 \to +\infty} \left[\boldsymbol{v}^1(\mathbf{y}, x_2, \tau) - y_1 \dfrac{\partial \boldsymbol{u}^0}{\partial x_1}(0^+, x_2, \tau) \right]. & \text{(23b)} \end{cases}$$

Obviously, symmetrical expressions would be obtained if $y_1 = 0$ was chosen symmetrically, but the same final jump conditions would be obtained.

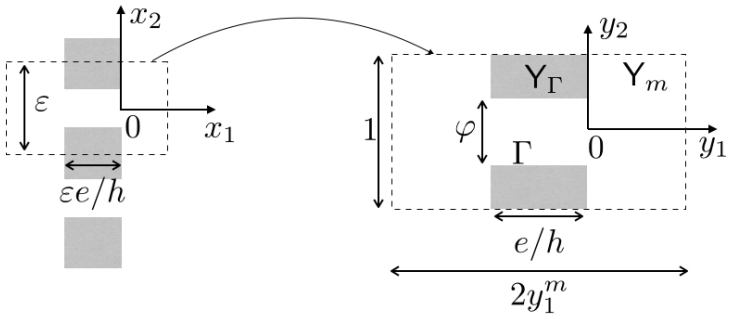

FIG. 4. The structured array in the two systems of coordinates $\mathbf{x}$ and $\mathbf{y}$. In $\mathbf{y}$- coordinate, Y_Γ and Y_m are the domains occupied by the rigid inclusions and by the air respectively ($\mathsf{Y} = \lim_{y_1^m \to +\infty} \mathsf{Y}_m$); Γ is the boundary of Y_Γ where Neumann boundary condition applies ($\mathcal{S}_c = e\varphi/h$ is the surface of air within the array).

We define $\mathsf{Y}_m^t = (-y_1^m, y_1^m) \times (-1/2, 1/2)$, and as previously, Y_Γ and Y_m are the domains occupied by the rigid inclusions and by the air in Y_m^t; Neumann boundary conditions apply on the boundary Γ of Y_Γ in contact with the air. The unit cell corresponds to $\mathsf{Y} = \lim_{y_1^m \to \infty} \mathsf{Y}_m$. Inside Y, the air groove has a thickness e/h along y_1 and a height φ along y_2; we denote $\mathcal{S}_c = e\varphi/h$ the corresponding surface.

1. Solution at order 0

As for the structured surface, the Eq. (7a) tells us that q^0 does not depend on $\mathbf{y}$, and from Eq. (21a), $q^0(x_2, \tau) = p^0(0^\pm, x_2, \tau)$. Next, Eq. (7b) is integrated in Y leading to $\int_{-1/2}^{1/2} \mathrm{d}y_2 \, [v_1^0(+\infty, y_2, x_2, \tau) - v_1^0(-\infty, y_2, x_2, \tau)] = 0$, and from Eq. (21b), $u_1^0(0^\pm, \tau) = \int_{-1/2}^{1/2} \mathrm{d}y_2 \, v_1^0(\pm\infty, y_2, x_2, \tau)$. Thus, the jump conditions read

$$[\![p^0]\!] = 0, \quad [\![u_1^0]\!] = 0.$$

At the leading order, the film is transparent for the waves and again, we need to go at the next order to capture the effect of the microstructure. Before doing so, we have to define the elementary problems which make the interface parameters to appear.

2. Solution at order 1and Elementary problems

To define the elementary problem, we start from the system of Eqs. (12) which is still valid but it does not simplify since $u_1^0(0, x_2, \tau)$ is unknown. The system of Eqs. (12) is now linear with respect to both components of $\boldsymbol{\nabla}_{\mathbf{x}} p^0(0, x_2, \tau)$. Thus, we need two elementary solutions $Q^{(i)}(\mathbf{y})$, $i = 1, 2$, with

$$q^1 = \frac{\partial p^0}{\partial x_1}(0, x_2, \tau) Q^{(1)}(\mathbf{y}) + \frac{\partial p^0}{\partial x_2}(0, x_2, \tau) Q^{(2)}(\mathbf{y}) + Q(\mathbf{x}, \tau), \tag{24}$$

and $Q^{(i)}$ satisfying

$$\begin{cases} \Delta Q^{(1)} = 0, \\ \boldsymbol{\nabla} Q^{(1)}.\mathbf{n}_{|\Gamma} = 0, \\ \lim\limits_{y_1 \to \pm\infty} \boldsymbol{\nabla} Q^{(1)} = \mathbf{e}_1, \end{cases} \qquad \begin{cases} \Delta Q^{(2)} = 0, \\ \left[\mathbf{e}_2 + \boldsymbol{\nabla} Q^{(2)}\right].\mathbf{n}_{|\Gamma} = 0, \\ \lim\limits_{y_1 \to \pm\infty} \boldsymbol{\nabla} Q^{(2)} = \mathbf{0}. \end{cases} \tag{25}$$

$Q^{(1)}$ is of the form

$$Q^{(1)}(\mathbf{y}) = \begin{cases} y_1 + Q_{\text{ev}}, & y_1 < 0, \\ y_1 + \mathcal{B} + Q_{\text{ev}} & y_1 > 0, \end{cases} \tag{26}$$

with Q_{ev} an evanescent field, vanishing at $\pm\infty$. Now, we use (for the first time) the symmetry of the inclusions *w.r.t.* y_2 to conclude that $Q^{(2)}$ vanishes at $y_1 \to \pm\infty$. Indeed, the symmetry imposes $Q^{(2)}$ to be odd *w.r.t.* y_2, whence $Q^{(2)}(y_1, 0) = 0$ and $Q^{(2)} \to 0$ at $y_1 \to \pm\infty$. Both $Q^{(1)}$ and $Q^{(2)}$ are related to problems of fluid mechanics and this is discussed in the Appendix A. As previously, $Q(\mathbf{x}, \tau)$ has been introduced since the Eqs. (12) define q^1 up to a function independent of $\mathbf{y}$, and as previously, it will not be necessary to determine it.

3. Jump condition at the equivalent interface

We can now inspect the solution at order 1. From the matching conditions, Eqs. (22a) and (23a), we get the jump in p^1 using the Eq. (24)

$$[\![p^1]\!] = \left(\mathcal{B} + \frac{e}{h}\right) \frac{\partial p^0}{\partial x_1}(0, x_2, \tau).$$

To get the jump condition on u_1^1, we proceed in the same way as we did to get the Eqs. (16) - (17), with the extra term due to $Q^{(1)}$. It is easy to see that we get

$$\frac{\partial u_2^0}{\partial x_2}(0,x_2,\tau)\int_{\mathsf{Y}_m}\mathrm{d}\mathbf{y}\ \frac{\partial Q^{(2)}}{\partial y_2}+\mathcal{S}\ \frac{\partial u_1^0}{\partial x_1}(0,x_2,\tau)+\int_{-1/2}^{1/2}\mathrm{d}y_2\left[v_1^1(y_1^m)-v_1^1(-y_1^m)-2y_1^m\frac{\partial u_1^0}{\partial x_1}(0,x_2,\tau)\right]=0,$$

(similar to Eq. (17)). We have used that the surface of Y_m is $(2y_1^m-\mathcal{S})$, with $\mathcal{S}$ the surface fraction of the inclusions (and thus $\mathcal{S}+\mathcal{S}_c=e/h$). We have also used the symmetry of the inclusion: with $Q^{(1)}$ being symmetric *w.r.t.* y_2, the integral of $\partial_{y_2}Q^{(1)}$ vanishes. To conclude on the jump in u_1^1, it is sufficient to recognize the matching conditions Eqs. (22b) and (23b) in the last integral over y_2 for $y_1^m\to+\infty$, namely

$$\lim_{y_1^m\to+\infty}\int_{-1/2}^{1/2}\mathrm{d}y_2\left[v_1^1(-y_1^m)+y_1^m\ \frac{\partial u_1^0}{\partial x_1}(0,x_2,\tau)\right]=u_1^1(0^-,x_2,\tau)+\frac{e}{h}\ \frac{\partial u_1^0}{\partial x_1}(0,x_2,\tau),$$
$$\lim_{y_1^m\to+\infty}\int_{-1/2}^{1/2}\mathrm{d}y_2\left[v_1^1(y_1^m)-y_1^m\ \frac{\partial u_1^0}{\partial x_1}(0,x_2,\tau)\right]=u_1^1(0^+,x_2,\tau).$$

We get the final jump conditions

$$[\![u_1^1]\!]=\mathcal{S}_c\ \frac{\partial u_1^0}{\partial x_1}(0,x_2,\tau)+\mathcal{C}\ \frac{\partial u_2^0}{\partial x_2}(0,x_2,\tau),$$

with the same definition of $\mathcal{C}$ as in Eq. (18) (but not the same value, the elementary problems on $Q^{(2)}$ being different). We have also used that $\mathcal{S}_c=(e/h-\mathcal{S})$. Finally, with $[\![p]\!]=\varepsilon\,[\![p^1]\!]+O(\varepsilon^2)$ and $p=p^0+O(\varepsilon)$ (the same for u_1), and coming back to the real space, the jump conditions at the equivalent interface of thickness e read

$$\begin{cases}[\![P]\!]=(e+h\mathcal{B})\ \overline{\dfrac{\partial P}{\partial X_1}},\\[2ex] [\![U_1]\!]=e\varphi\ \overline{\dfrac{\partial U_1}{\partial X_1}}+h\mathcal{C}\ \overline{\dfrac{\partial U_2}{\partial X_2}},\end{cases}\tag{27}$$

where we used $\mathcal{S}_c=\varphi e/h$.

B. Energy conservation for the equivalent thin interface

It is now possible to write the equation of energy conservation in the homogenized problem. In this problem, the domain between $-e$ and 0 is not considered. If we have numerical implementations in mind, this domain would be not considered, and the jump conditions, Eqs. (27), would apply between $X_1=-e$ and $X_1=0$ (Fig. 5). Now the boundary $\partial\Omega$ of Ω

includes the planes $X_1 = -e$ and $X_1 = 0$. In the real problem, the acoustic energy in the region sandwiched between these two planes reads

$$\int_{\Omega_e} dV \ \left[\frac{\rho_0}{2}U^2 + \frac{\chi_0}{2}P^2\right],$$

while in the homogenized problem, it is handled by the thin interface through the last integral in the equation of energy conservation below

$$\frac{d}{dt}\mathcal{E} = \frac{d}{dt}\int_{\Omega\backslash\Omega_e} dV \ \left[\frac{\rho_0}{2}U^2 + \frac{\chi_0}{2}P^2\right] - \int \mathrm{d}X_2 \ [\![PU_1]\!].$$

As previously, the term $I \equiv -\int \mathrm{d}X_2 \ [\![PU_1]\!]$ has to be the time derivative of a positive quantity. With $[\![PU_1]\!] = [\![P]\!]\,\overline{U_1} + \overline{P}\,[\![U_1]\!]$, and applying the jump conditions, Eqs. (27), we get

$$I = -\int \mathrm{d}X_2 \left[(e + h\mathcal{B}) \ \overline{\frac{\partial P}{\partial X_1}}\ \overline{U_1} + h\mathcal{S}_c\,\overline{P}\ \overline{\frac{\partial U_1}{\partial X_1}} + h\mathcal{C}\,\overline{P}\ \overline{\frac{\partial U_2}{\partial X_2}}\right].$$

Next, we use the Eqs. (1) to get

$$I = \frac{d}{dt}\mathcal{E}_s, \quad \mathcal{E}_s = \int \mathrm{d}X_2 \left[\frac{\rho_0}{2}\left((e + h\mathcal{B})\ \overline{U_1}^2 + (e\varphi - h\mathcal{C})\ \overline{U_2}^2\right) + \frac{\chi_0}{2}e\varphi\ \overline{P}^2\right]. \tag{28}$$

Here, the parameter $e\varphi$ (in the coefficients associated to U_2^2 and P^2) has appeared because the interface thickness has been set equal to e. If the jump conditions at a zero thickness interface were used, we would get a coefficient associated to U_2^2 equal to $-h(\mathcal{C} + \mathcal{S}) < 0$ (because $\mathcal{C} > 0$, see Appendix B) and a coefficient associated to P^2 equal to $-\mathcal{S} < 0$, which is not really suitable for a term of energy and not suitable at all for numerical purpose.

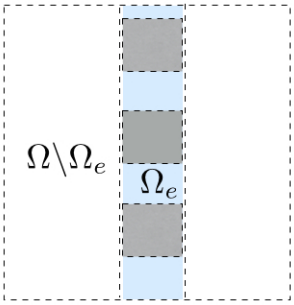

FIG. 5. The domain Ω in the actual problem with the structured film will be replaced by the domain $\Omega\backslash\Omega_e$ in the homogenized problem.

IV. TWO -STEP HOMOGENIZATION USING CLASSICAL HOMOGENIZATION OF BULK MATERIAL

As previously said, the classical homogenization has been shown to capture accurately the behavior of micro-structured material and it is tempting to see how it compares with the interface homogenization for surfaces or films of small thicknesses. This is not to inspect whether or not the classical homogenization resists in this limit, since we already know that it fails when $ke < 1$, see [19]. The goal in this section is rather to get insight into what causes this failure. This is done following [24] using a two-step homogenization. We start by recalling the derivation of the effective parameters in the classical homogenization; this is the first step homogenization, leading to an equivalent anisotropic layer, with effective mass density and bulk modulus, being explicit for rigid layers (they will be function of φ only). The second step consists in determining the equivalent boundary condition or jump conditions when the layer thickness vanishes and this will be done by applying a matched asymptotic expansion technique.

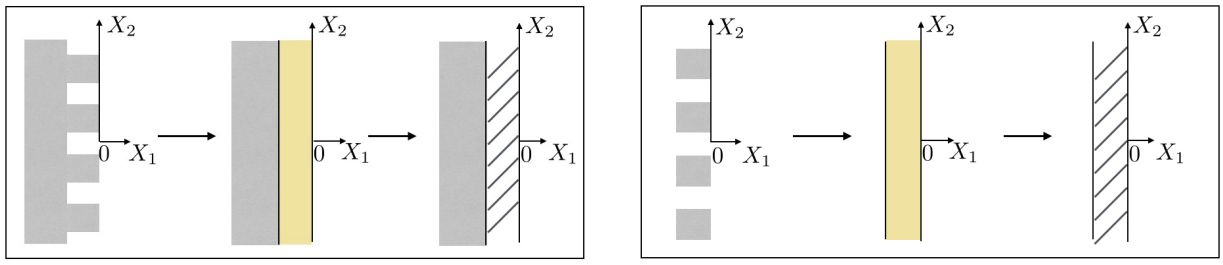

(a) (b)

FIG. 6. Two-step homogenization with classical homogenization in the first step, leading to an equivalent homogeneous anisotropic layer, and in the second step, matched asymptotic expansions leading to (a) an equivalent boundary condition at $X_1 = 0$, (b) equivalent jump conditions across the equivalent thin interface bounded by $X_1 = -e$ and $X_1 = 0$.

A. First step homogenization, toward an equivalent anisotropic layer

The classical homogenization considers a structuration in the whole space. The expansion is done owing to a two scale expansions in $\mathbf{x}$ and now, $\mathbf{y} = \mathbf{x}/\varepsilon$

$$\begin{cases} p = q^0(\mathbf{y}, \mathbf{x}, \tau) + \varepsilon q^1(\mathbf{y}, \mathbf{x}, \tau) + \dots, \\ \\ \boldsymbol{u} = \boldsymbol{v}^0(\mathbf{y}, \mathbf{x}, \tau) + \varepsilon \boldsymbol{v}^1(\mathbf{y}, \mathbf{x}, \tau) + \dots \end{cases}$$

where the fields $(\boldsymbol{v}^n, q^n)$ are assumed to be periodic with respect to $\mathbf{y}$. The unit cell is now bounded along y_1 and y_2, of size 1^2, and in the unit cell, we define Y the region occupied by the air $\mathsf{Y} = (-1/2, 1/2) \times (-\varphi/2, \varphi/2)$; Neumann boundary conditions apply on Γ between the rigid layers and the air.

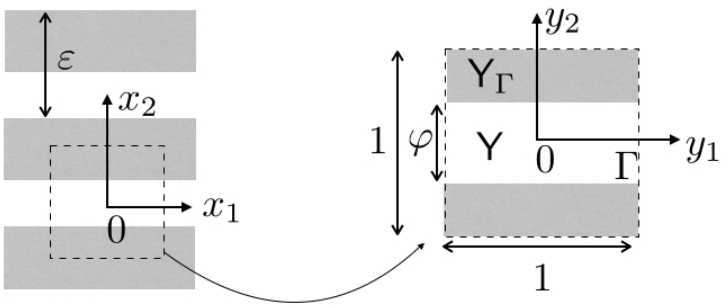

FIG. 7. In classical homogenization, the structuration occupies the whole space. The elementary problems are defined in the unit cell of size 1^2 in $\mathbf{y}$-coordinate and Y denotes the region occupied by the air; Γ are the boundaries of the rigid layers in contact with the air.

The expansions will be used in Eq. (2) at each order using the differential operator

$$\boldsymbol{\nabla} \to \frac{1}{\varepsilon}\boldsymbol{\nabla}_{\mathbf{y}} + \boldsymbol{\nabla}_{\mathbf{x}}.$$

The Eqs. (2) at order ε^{-1} read (i) $\boldsymbol{\nabla}_{\mathbf{y}} q^0 = 0$, from which q^0 depends on $(\mathbf{x}, \tau)$ only and (ii) $\mathrm{div}_{\mathbf{y}} \boldsymbol{v}^0 = 0$ that we shall use later. At order ε^0, the Eqs. (2) give

$$\begin{cases} \dfrac{\partial \boldsymbol{v}^0}{\partial \tau}(\mathbf{y}, \mathbf{x}, \tau) = -\boldsymbol{\nabla}_{\mathbf{x}} q^0(\mathbf{x}, \tau) - \boldsymbol{\nabla}_{\mathbf{y}} q^1(\mathbf{y}, \mathbf{x}, \tau), \\ \dfrac{\partial q^0}{\partial \tau}(\mathbf{x}, \tau) + \mathrm{div}_{\mathbf{x}} \boldsymbol{v}^0(\mathbf{y}, \mathbf{x}, \tau) + \mathrm{div}_{\mathbf{y}} \boldsymbol{v}^1(\mathbf{y}, \mathbf{x}, \tau) = 0. \end{cases} \tag{29}$$

These two equations will be averaged in Y, which will make a wave equation to appear for the two fields $\int_{\mathsf{Y}} \mathrm{d}\mathbf{y}\ \boldsymbol{v}^0(\mathbf{y},\mathbf{x},\tau)$ and $q^0(\mathbf{x},\tau)$. Contrary to the interface homogenization, the classical homogenization yields the equivalent medium at the leading order in the expansion.

As in the interface homogenization, elementary problems are needed to get the parameters of the equivalent medium. To get them, we use the time derivative versions of $\mathrm{div}_{\mathbf{y}}\boldsymbol{v}^0 = 0$ and of the boundary condition $\boldsymbol{v}^0.\mathbf{n}_{|\Gamma} = 0$. From the first equation in Eqs. (29), we find that (q^0, q^1) satisfy

$$\begin{cases} \Delta_{\mathbf{y}} q^1(\mathbf{y},\mathbf{x},\tau) = 0, \\ \\ \left[\boldsymbol{\nabla}_{\mathbf{y}} q^1(\mathbf{y},\mathbf{x},\tau) + \boldsymbol{\nabla}_{\mathbf{x}} q^0(\mathbf{x},\tau)\right].\mathbf{n}_{|\Gamma} = 0. \end{cases}$$

Next, by linearity of the above system, it is possible to define

$$q^1(\mathbf{y},\mathbf{x},\tau) = \frac{\partial q^0}{\partial x_1}(\mathbf{x},\tau) Q^{(1)}(\mathbf{y}) + \frac{\partial q^0}{\partial x_2}(\mathbf{x},\tau) Q^{(2)}(\mathbf{y}) + Q(\mathbf{x},\tau), \tag{30}$$

with $Q^{(i)}(\mathbf{y})$ satisfying the elementary problems

$$\begin{cases} \Delta Q^{(i)} = 0, \\ \\ \left[\mathbf{e}_i + \boldsymbol{\nabla} Q^{(i)}\right].\mathbf{n}_{|\Gamma} = 0. \end{cases} \tag{31}$$

Once the elementary problems are solved, it is sufficient to use Eq. (30) in Eqs. (29) being integrated over Y. With $p(\mathbf{x},\tau) = q^0(\mathbf{x},\tau)$ and $\boldsymbol{u}(\mathbf{x},\tau) = \int_{\mathsf{Y}} \mathrm{d}\mathbf{y}\ \boldsymbol{v}^0(\mathbf{y},\mathbf{x},\tau)$ at the dominant order, we get

$$\begin{cases} \dfrac{\partial \boldsymbol{u}}{\partial \tau} = -\mathsf{A}\boldsymbol{\nabla}_{\mathbf{x}} p, \\ \\ \varphi\ \dfrac{\partial p}{\partial \tau} + \mathrm{div}_{\mathbf{x}}\boldsymbol{v} = 0, \end{cases} \tag{32}$$

with φ the surface of Y and

$$\mathsf{A}_{ij} \equiv \int \mathrm{d}\mathbf{y}\ \left[\boldsymbol{\nabla} Q^{(j)} + \mathbf{e}_j\right] \mathbf{e}_i.$$

We have used the periodicity of $\boldsymbol{v}^1$ *w.r.t.* $\mathbf{y}$ and the boundary conditions $\boldsymbol{v}^1.\mathbf{n}_{|\Gamma} = 0$ to get $\int_{\mathsf{Y}} \mathrm{d}\mathbf{y}\ \mathrm{div}_{\mathbf{y}}\boldsymbol{v}^1(\mathbf{y},\mathbf{x},\tau) = 0$. Coming back to the real space, we get the homogenized wave equation

$$\begin{cases} \rho_0 \dfrac{\partial \boldsymbol{U}}{\partial t} = -\mathsf{A}\boldsymbol{\nabla} P, \\ \\ \chi_0 \varphi\ \dfrac{\partial P}{\partial t} + \mathrm{div}\boldsymbol{U} = 0, \end{cases} \tag{33}$$

which corresponds to an equivalent homogeneous and anisotropic medium, with an effective inverse mass density tensor $\rho_0^{-1}\mathsf{A}$ and an effective compressibility $\chi_0\varphi$. Again, the elementary

problems, Eqs. (31), correspond to problems of perfect fluids flowing around obstacles, but in the present case, the solutions are intuitively trivial (and mathematically also in fact), leading to $Q^{(1)} = 0$ and $Q^{(2)} = -y_2$ (see Appendix A). The matrix A is thus reduced to

$$\mathsf{A} = \begin{pmatrix} \varphi & 0 \\ 0 & 0 \end{pmatrix}. \tag{34}$$

B. Second step -homogenization

We assume that the homogenization in the first step is legitimate even when the thickness e of the equivalent layer is smaller than the typical wavelength $1/k$, and we define $\varepsilon' \equiv ke \ll 1$. Then, we can determine the boundary condition (for the layer being on a rigid wall), or the jump conditions (for the layer being placed in air), following the matched asymptotic expansion presented in [22] and the procedure is very similar to the one developed for the homogenization in Sec. III.

As previously, two different (outer and inner) expansions are used with respect to the new small parameter ε'; a significant simplification comes from the fact that there is no structuration along y_2 anymore, and thus no need in the coordinate y_2 (in fact, the problem is one -dimensional now). Thus, the inner expansions are written as

$$\text{Inner exp.} \begin{cases} p = q^0(y_1, x_2, \tau) + \varepsilon' q^1(y_1, x_2, \tau) + \ldots, \\ \\ \boldsymbol{u} = \boldsymbol{v}^0(y_1, x_2, \tau) + \varepsilon' \boldsymbol{v}^1(y_1, x_2, \tau) + \ldots \end{cases}$$

while the outer expansions remain the same as in Eq. (4). The wave propagation in the succession of media $(\Omega^-, \Omega, \Omega^+)$ (Fig. 8), is described by

$$\begin{cases} \dfrac{\partial \boldsymbol{u}}{\partial \tau} = -\mathsf{a} \boldsymbol{\nabla} p, \\ \\ b \dfrac{\partial p}{\partial \tau} + \mathrm{div} \boldsymbol{v} = 0. \end{cases} \tag{35}$$

In the inner problem, a and b depend on y_1. In the outer problem, they depend on x_1 being piecewise constant in $\Omega^{\pm}$ (Fig. 8). For a structured wall, Ω^- is a rigid wall, for a structured film, it is the air. In both cases, Ω^+ is the air. These equations will be written at each order in the outer and inner regions owing to the expressions of the differential operator

$$\begin{cases} \boldsymbol{\nabla} \to \boldsymbol{\nabla}_{\mathbf{x}}, \quad \text{in the outer problem,} \\ \boldsymbol{\nabla} \to \dfrac{1}{\varepsilon'} \dfrac{\partial}{\partial y_1} \mathbf{e}_1 + \dfrac{\partial}{\partial x_2} \mathbf{e}_2, \quad \text{in the inner problem.} \end{cases}$$

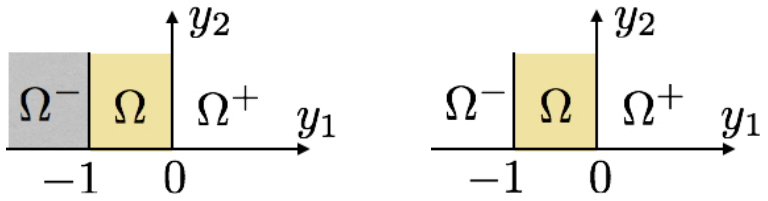

(a) (b)

FIG. 8. In the second step homogenization, the layer Ω in $\mathbf{y}$ coordinates occupies $-1 < y_1 < 0$, (a) with Ω^- being a rigid wall and (b) with Ω^- being the air.

1. Ω^- is a rigid wall

In the inner region, we start with the leading order of (35) in $1/\varepsilon'$: $\partial_{y_1} q^0 = \partial_{y_1} v_1^0 = 0$, from which $p^0(0, x_2, \tau) = q^0(x_2, \tau)$ and $u_1^0(0, x_2, \tau) = v_1^0(x_2, \tau)$. Accounting for these relations, Eqs. (35) at order $(\varepsilon')^0$ read

$$\begin{cases} \dfrac{\partial u_1^0}{\partial \tau}(0, x_2, \tau) = -a_1(y_1)\, \dfrac{\partial q^1}{\partial y_1}, & \text{(36a)} \\ \dfrac{\partial v_2^0}{\partial \tau} = -a_2(y_1)\, \dfrac{\partial p^0}{\partial x_2}(0, x_2, \tau), & \text{(36b)} \\ b(y_1)\, \dfrac{\partial p_0}{\partial \tau}(0, x_2, \tau) + \dfrac{\partial v_2^0}{\partial x_2} + \dfrac{\partial v_1^1}{\partial y_1} = 0, & \text{(36c)} \end{cases}$$

and when non specified, the functions have a dependence in the coordinates (y_1, x_2, τ). In the above expressions, the coefficients $a_1(y_1)$ and $a_2(y_1)$ are the diagonal terms of $\mathsf{a}(y_1)$; the generalization to a non diagonal matrix a is rather straightforward, but not very useful for the present purpose. The coefficients (a_1, a_2, b) are piecewise constant, with $a_1 = \varphi$, $a_2 = 0$, $b = \varphi$ for $-1 < y_1 < 0$ (from the first step homogenization), and $a_1 = a_2 = b = 1$ for $y_1 > 0$ (being the air). Next, Ω^- is not considered, but Neumann boundary condition applies at $y_1 = -1$.

As for the interface homogenization, a boundary condition on the velocity is sought, and because $v_1^0(x_2, \tau)$ does not depend on y_1, it starts with $0 = v_1^0(x_2, \tau) = u_1^0(0, x_2, \tau)$, imposed by the Neumann boundary condition at $y_1 = -1$ at order 0 for the inner solution. The matching condition at order 1 is the same as Eq. (10) (with $\mathbf{y} \to y_2$ in the present case); it is written in a slightly different, but equivalent, form below

$$u_1^1(0, x_2, \tau) = \lim_{y_1 \to +\infty} \left\{ \int_{-1}^{0} \mathrm{d}y \frac{\partial v_1^1}{\partial y}(y, x_2, \tau) \; + \int_{0}^{y_1} \mathrm{d}y \; \left[\frac{\partial v_1^1}{\partial y}(y, x_2, \tau) - \frac{\partial u_1^0}{\partial x_1}(0, x_2) \right] \right\}, \quad (37)$$

where we have used the boundary condition $v_1^1(-1, x_2, \tau) = 0$ on the rigid wall. Next, we shall determine $\partial_y v_1^1$ in each integral. To begin with, the time derivative of Eq. (36c), with Eq. (36b), gives

$$\frac{\partial}{\partial \tau}\frac{\partial v_1^1}{\partial y_1} = a_2 \, \frac{\partial^2 p^0}{\partial x_2^2}(0, x_2, \tau) - b \, \frac{\partial^2 p^0}{\partial \tau^2}(0, x_2, \tau),$$

and the above equation is valid for $y_1 > -1$. From the outer region, Eqs. (35) with $\mathsf{a} = 1$ and $b = 1$, we have $\partial_{x_2} p^0(0, x_2) = -\partial_\tau u_2^0(0, x_2)$ and $\partial_\tau p^0(0, x_2) = -\mathrm{div}_{\mathbf{x}} \boldsymbol{u}^0(0, x_2)$, from which

$$\frac{\partial v_1^1}{\partial y_1} = b \, \frac{\partial u_1^0}{\partial x_1}(0, x_2, \tau) + (b - a_2) \, \frac{\partial u_2^0}{\partial x_2}(0, x_2, \tau), \tag{38}$$

where only b and a_2 are function of y_1 in the right hand side terms of Eq. (38). The Eq. (38) holds in Ω and in Ω^+ and it can be used to evaluate the two integrals in the Eq. (37): the first integral is obtained with $b = \varphi$ and $a_2 = 0$, and the second integral vanishes since $b = a_2 = 1$. Finally, we obtain

$$u_1^1(0, x_2, \tau) = \varphi \, \mathrm{div}_{\mathbf{x}} \boldsymbol{u}^0(0, x_2, \tau),$$

and coming back to the real space at dominant order (with $\varepsilon' = ke$)

$$U_1(0, X_2, t) = e\varphi \left[\frac{\partial U_1}{\partial X_1}(0, X_2, t) + \frac{\partial U_2}{\partial X_2}(0, X_2, t) \right], \tag{39}$$

and the above boundary condition has to be compared with Eq. (19).

2. Ω^- is the air

The calculation for a layer (Fig. 8(b)) is straightforward thanks to the previous calculation. Here, we want to derive jump conditions, and this starts with $[\![u_1^0]\!] = [\![p^0]\!] = 0$ because $v_1^0(x_2, \tau) = u^0(0^\pm, x_2, \tau)$ and $q^0(x_2, \tau) = p^0(0^\pm, x_2, \tau)$. The jump in p^1 and u_1^1 are obtained following the same technique as in the preceding section. As previously, the jumps are defined using the matching conditions, similar to those in Eqs. (22)-(23); but now, because the expansions has been performed *w.r.t* $\varepsilon' = \varepsilon(e/h)$, the y_1-translation for Ω^- is of unity instead of being of e/h. Thus, the matching conditions are the same than in Eqs. (22)-(23) setting e/h to unity (and again $\mathbf{y} \to y_2$ in these expressions). They are written below in an

equivalent form

$$\begin{cases} [\![p^1]\!] = \lim\limits_{y_1\to+\infty}\left\{\displaystyle\int_{-1}^{0}\mathrm{d}y\frac{\partial q^1}{\partial y}+\int_{0}^{y_1}\mathrm{d}y\ \left[\frac{\partial q^1}{\partial y}-\frac{\partial p^0}{\partial x_1}(0^+,x_2)\right]+\int_{-y_1}^{-1}\mathrm{d}y\ \left[\frac{\partial q^1}{\partial y}-\frac{\partial p^0}{\partial x_1}(0^-,x_2)\right]\right\}, \\ [\![u_1^1]\!] = \lim\limits_{y_1\to+\infty}\left\{\displaystyle\int_{-1}^{0}\mathrm{d}y\frac{\partial v_1^1}{\partial y}+\int_{0}^{y_1}\mathrm{d}y\ \left[\frac{\partial v_1^1}{\partial y}-\frac{\partial u_1^0}{\partial x_1}(0^+,x_2)\right]+\int_{-y_1}^{-1}\mathrm{d}y\ \left[\frac{\partial v_1^1}{\partial y}-\frac{\partial u_1^0}{\partial x_1}(0^-,x_2)\right]\right\}. \end{cases} \tag{40a}$$

(40b)

For the calculation of $[\![u_1^1]\!]$, almost everything has been done in the previous section; it is sufficient to use Eq. (38) with $a_2 = b = 1$ for $y_1 < -1$ (being now the air) to find that the last integral of Eq. (40b) vanishes (and the two first integrals are the same than previously). To get $[\![p^1]\!]$, we use Eq. (36a), and owing to $\partial_\tau u_1^0(0,x_2,\tau) = -\partial_{x_1} p^0(0,x_2,\tau)$ from the outer region, we have

$$\frac{\partial q^1}{\partial y_1} = \frac{1}{a_1}\frac{\partial p^0}{\partial x_1}(0^\pm,x_2,\tau).$$

Again, only a_1 depends on y_1 in the right hand side term of the above equation. With $a_1 = 1$ for $y_1 < -1$ and $y_1 > 0$ and with $a_1 = \varphi$ for $-1 < y_1 < 0$, only the fist integral in Eq. (40a) has a non vanishing contribution and we get the two jump conditions, written below in the real space

$$\begin{cases} [\![P]\!] = \dfrac{e}{\varphi}\,\overline{\dfrac{\partial P}{\partial X_1}}, \\ [\![U_1]\!] = e\varphi\left[\overline{\dfrac{\partial U_1}{\partial X_1}}+\overline{\dfrac{\partial U_2}{\partial X_2}}\right]. \end{cases} \tag{41}$$

The above jump conditions have to be compared with those in Eqs. (27).

C. Comparison of the two homogenizations – What is wrong ?

The boundary conditions in Eqs. (19) and (39) and the jump conditions in Eqs. (27) and (41) have the same structures but they do not involve the same parameters. The case of rectangular inclusions is enlighting for the comparison, since explicit expression of $\mathcal{B}$ is available

$$\mathcal{B} = \frac{e}{h}\frac{1-\varphi}{\varphi}+\mathcal{B}_0, \quad \mathcal{B}_0 = \frac{2}{\pi}\log\left(\sin\frac{\pi\varphi}{2}\right)^{-1},$$

and the second contribution $\mathcal{B}_0$ corresponds to flat rigid plates ($e = 0$). Let us now re-write the boundary condition and the jump conditions coming from the interface homogenization

$$U_1(0, X_2, t) = e\varphi \frac{\partial U_1}{\partial X_1}(0, X_2, t) + h\mathcal{C} \frac{\partial U_2}{\partial X_2}(0, X_2, t). \tag{42}$$

$$\begin{cases} [\![P]\!] = \left(\dfrac{e}{\varphi} + \mathcal{B}_0 \right) \overline{\dfrac{\partial P}{\partial X_1}}, \\ [\![U_1]\!] = e\varphi \overline{\dfrac{\partial U_1}{\partial X_1}} + h\mathcal{C} \overline{\dfrac{\partial U_2}{\partial X_2}}. \end{cases} \tag{43}$$

By inspection of the expressions in Eqs. (39) and (41) and their comparison with the above expressions, the questions are clear:

- is $\mathcal{B}_0$ negligible compared to $e\varphi/h$?
- how close from $e\varphi/h$ is $\mathcal{C}$?

The first question is easy to answer, since $\mathcal{B}_0$ is independent of e. Thus, increasing e makes the first condition more and more fulfilled and reversely, vanishing thickness of the interface produces a significant error in the two-step homogenization prediction. Classical homogenization leads to a homogenized equivalent layer, and vanishing layer thickness produces a vanishing effect, by construction; this has to be contrasted with the real structuration with vanishing thickness: flat rigid plates obviously are able to scatter waves. This has to be related with the equivalent elementary problem appearing in the interface homogenization: $Q^{(1)}$ satisfies Eqs. (25) and it is the velocity potential associated to a perfect fluid flowing in a duct obstructed by a rigid obstacle; for vanishing thickness, the obstacle still deviates the flow, resulting in a non vanishing $Q^{(1)}$, and thus a non vanishing $\mathcal{B}$ (see Appendix A).

The second question is more involved because an explicit expression of $\mathcal{C}$ is not available. The parameter $\mathcal{C}$ is also related to a fluid mechanics problem. It is the mean value of the perturbation velocity along $\mathbf{e}_2$ inside the grooves, for a potential flow flowing along $\mathbf{e}_2$ with velocity unity far from the structuration ($\mathbf{u} = \mathbf{e}_2 + \boldsymbol{\nabla} Q^{(2)}$ in Eqs. (25), see also Appendix A). Obviously, in the absence of structuration ($e = 0$), the velocity along $\mathbf{e}_2$ equals unity everywhere and $e = h\mathcal{C} = 0$. Consider now the limit where e becomes larger than the groove height $h\varphi$. In this case, we do not expect the flow to enter deeply inside the grooves. This is illustrated in Fig. 9(a) where we reported the fields of $\mathbf{u}.\mathbf{e}_2$ computed for $e/h = 2$ and 4;

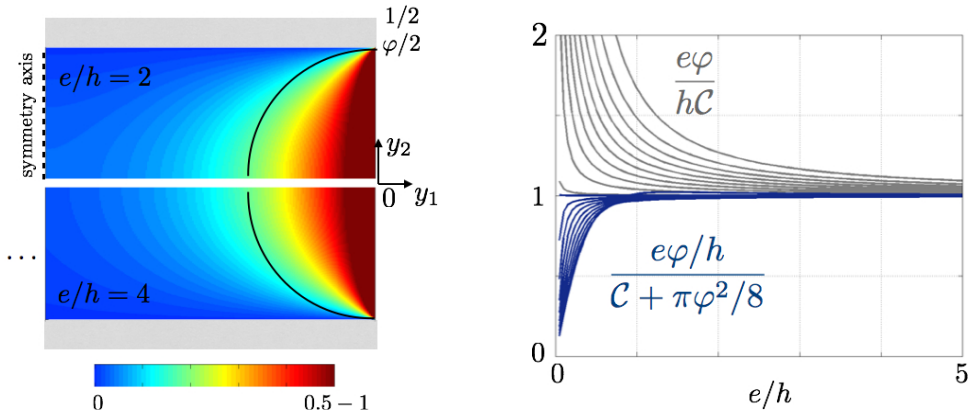

(a) (b)

FIG. 9. (a) Fields of the velocity component $\mathbf{u}.\mathbf{e}_2 = 1+\partial_{y_2}Q^{(2)}$ inside the grooves. The calculation is done solving Eqs. (25). The reported results correspond to $\varphi = 0.8$ and $e/h = 2$ (upper panel) and $e/h = 4$ (bottom panel); the black lines show $\sqrt{y_1^2+y_2^2} = \varphi/2$. (b) Inspection of the bounds for $\mathcal{C}$ (various $0 < \varphi < 1$ are collected).

the calculations are presented in the case of a structured array. The two flows are similar, being essentially confined in a boundary layers near $y_1 = 0$, in the half disc of radius $\varphi/2$. Thus, a rough estimate can be done according to

$$\text{for } e/h > \varphi/2, \quad \int_{\text{groove}} \mathrm{d}\mathbf{y}\ \mathbf{u}.\mathbf{e}_2 \simeq \frac{1}{2}\int_{(y_1^2+y_2^2)<\varphi^2/4} \mathrm{d}\mathbf{y}\ \ 1 = \frac{\pi}{8}\varphi^2,$$

(where the mean velocity has been set to 1/2 and accounting for the two boundary layers in the case of the array). This behavior is confirmed in Fig. 9(b), together with the condition $h\mathcal{C} < e\varphi$ (which is a good news for the surface and interface energies in Eqs. (20) and (28)). From Fig. 9(b), we get bounds for $\mathcal{C}$

$$\frac{e\varphi}{h} - \frac{\pi}{8}\varphi^2 < \mathcal{C} < \frac{e}{h}\varphi, \tag{44}$$

from which $\mathcal{C} \to e/h$ for large e/h. For small e/h values, $\mathcal{C}$ remains positive and vanishes faster than e, resulting again in a failure of the two step homogenization.

Our analysis of the $\mathcal{B}$- and $\mathcal{C}$-parameters is restricted to the case of rectangular shape structuration. What remains valid for any shapes is the limit for $e \to 0$: there, $\mathcal{B} \to \mathcal{B}_0$ will be always observed (because all the shapes end in flat plates for $e = 0$), and because $\mathcal{B}_0$ is significant for small φ, significant differences can be observed [19]. What will probably remains valid as well is the shift between $\mathcal{C}$ and e/h (which means that the vertical velocity

inside the grooves is not accelerated). But as $\mathcal{C}$ and e/h both vanish, the differences are less impressive and this has been checked (results are not reported here). In other words, vanishing roughnesses on a rigid wall lead to vanishing effects on the waves, while a vanishing thickness of a rigid array continues to efficiently scatter waves.

V. CONCLUDING REMARKS

In this paper, we have presented an interface homogenization for acoustic waves in the time domain; the case of thin periodic roughnesses on a wall and the case of a thin structured array have been considered. We addressed the problem of the acoustic energy associated to the equivalent wall or associated to the equivalent interface. It has been shown that the position of this wall or the thickness of this interface are not incidental (even if the conditions for any position or any thickness are equivalent up to the second order). If we have in mind the numerical implementation of the homogenized problem, this is crucial since it determines the stability of the numerical scheme. This is in fact not incidental neither in the frequency domain where the validity of the homogenized prediction may be extended significantly up to $ke \simeq 1$ when using the conditions presented in this paper, and this will be exemplified elsewhere.

Next, we have examined the failure of the classical homogenization in the limit of small thicknesses; for rigid materials, it will always fails. If the two-step homogenization theory resists to the limit $e \to 0$, we can guess that no significant effect will be observed. This is because the classical homogenization predicts vanishing effective parameters for vanishing thicknesses (by construction). To anticipate if vanishing thicknesses can lead to unexpected effects (and thus possibly to "extraordinary" propagations), the analysis of the physical problems associated to the elementary problems is helpful (here, potential flows around obstacles, but they are also problems of heat conduction). Specifically, if the solutions of these problems do not involve significant boundary layer effects, vanishing thicknesses of the device will produce vanishing effective parameters, and nothing fantastic will happen. If bounds for these parameters can be found by means of mathematical considerations, our intuition of the associated physical problems are additional tools to go toward thin devices able to control the wave propagation in an unexpected way.

ACKNOWLEDGMENTS

J.-J.M thanks the support of the French Agence Nationale de la Recherche (ANR), under grant Aramis (ANR-12-BS01-0021) Analysis of Robust Asymptotic Methods In numerical Simulation in mechanics. A.M. thanks B. Lombard for fruitful discussions.

Appendix A: The effective parameters

1. Remarks on the elementary problems

We have encountered four elementary problems (Fig. 10). All of them are of the same nature, namely, they are related to problems of perfect fluids flowing around rigid inclusions associated to Neumann boundary condition.

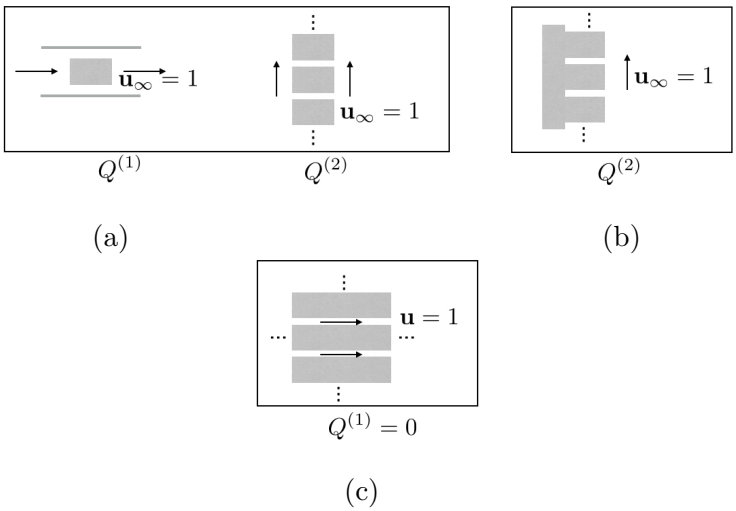

FIG. 10. The elementary problems appearing (a) for the structured rigid array, (b) for the structured rigid wall and (c) in the classical homogenization of rigid layers.

These are

1. $Q^{(1)}$ in Eqs. (26). It corresponds the potential flow past an obstacle in a channel. In this context, as in the context of breakwaters for water waves, this problem has been extensively studied in the literature, see *e.g* [14] and references herein. In these contexts, $\mathcal{B}$ is called the blockage coefficient, and its expression is known for several obstacle geometries (in an approximate of exact form).

2. $Q^{(2)}$ in Eqs. (15): it corresponds to a perfect fluid flowing along an infinite corrugated surface, with a velocity field $\mathbf{u} = \boldsymbol{\nabla} Q^{(2)} + \mathbf{u}_\infty$, and $\mathbf{u}_\infty = \mathbf{e}_2$. $Q^{(2)}$ is the perturbation velocity potential due to the corrugation. Next, it is easy to see that the coefficient $\mathcal{C} = -\int \mathrm{d}\mathbf{y}\ \partial_{y_2} Q^{(2)}$ has to be evaluated for $-e/h \leq y_1 \leq 0$ only (for $y_1 > 0$, $Q^{(2)}$ is periodic *w.r.t.* y_2 and thus, the integral vanishes). Thus, $\mathcal{C}$ appears to be the mean perturbation velocity along $\mathbf{e}_2$, $(\mathbf{u}_\infty - \mathbf{u}).\mathbf{e}_2$, in the grooves, but to the best of our knowledge, no explicit expression for $\mathcal{C}$ is available. We expect $\mathcal{C}$ to be positive (no acceleration in the grooves occurs) and smaller than unity (no reverse flow rate); next, the qualitative discussion in the Section IV, supported by numerical results (for a structured array), leads to the bounds, Eqs. (44). Finally, the value of $\mathcal{C}$ for the structured array (Fig. 10(a)) can be simply deduced from the value of $\mathcal{C}$ for the corrugated wall owing to the symmetry axis, and $\mathcal{C}_{\text{array}}(2e) = 2\mathcal{C}_{\text{wall}}(e)$.

3. $Q^{(1)}$ and $Q^{(2)}$ in the elementary problems appearing in the classical homogenization, Eq. (31). In the present case of rigid layers, these problems are trivial: $Q^{(1)}$ questions the perturbation velocity along $\mathbf{e}_1$ for a mean velocity being along $\mathbf{e}_1$; the flow is evidently not perturbed by the rigid layers, from which $Q^{(1)} = 0$. $Q^{(2)}$ questions the possibility for the fluid to flow along $\mathbf{e}_2$ and the answer is obviously that no flow is allowed in this direction. The total velocity has to cancel in the grooves, from which $Q^{(2)} = -y_2$. Also obvious is that $Q^{(1)} = 0$ and $Q^{(2)} = -y_2$ are exact solutions of Eqs. (31).

2. Simple procedure to get $\mathcal{C}$ for rectangular inclusions

Mode matching is a simple way to get $\mathcal{C}$. We consider the solution $Q = Q^{(2)} + y_2$ satisfying $\Delta Q = 0$, $\boldsymbol{\nabla} Q.\mathbf{n}_{|\Gamma} = 0$ and $Q \to y_2$ for $y_1 \to \infty$. The field Q can be written

$$Q(\mathbf{y}) = \begin{cases} Q^-(\mathbf{y}) = \displaystyle\sum_{n=1}^{N^-} q_n^- \frac{\cosh a_n(y_1+e)}{\cosh a_n e} f_n^-(y_2), \qquad 0 \geq y_1 \geq -e \\ Q^+(\mathbf{y}) = y_2 + \displaystyle\sum_{n=-N^+, n\neq 0}^{N^+} q_n^+ e^{-|b_n| y_1} f_n^+(y_2), \ y_1 \geq 0, \end{cases} \tag{A1}$$

with $a_n = n\pi/\varphi$, $b_n = 2n\pi$, and where

$$f_n^+(y_2) = e^{\mathrm{i} b_n y_2}, \quad f_n^-(y_2) = \sqrt{\frac{2-\delta_{n0}}{\varphi}} \cos\left(a_n y_2 + \frac{n\pi}{2}\right), \tag{A2}$$

are the transverse functions (forming a basis) adapted for solutions being respectively periodic and for solutions with zero derivatives at $y_2 = \pm\varphi/2$.

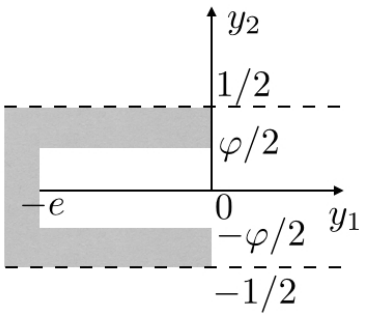

FIG. 11. Mode matching configuration. The solution $Q^{\pm}$ is written for $y_1 > -e$, and the resolution involves only matching conditions at $y_1 = 0$.

Now, we will ask to $Q^{\pm}$ to match (on average) their values and their first derivatives at $y_1 = 0$, and this latter matching on the derivatives will be done accounting for the Neumann boundary conditions at $y_1 = 0$ and $|y_2| > \varphi/2$ (note that Q^- satisfies by construction the Neumann boundary condition on at $y_2 = \pm\varphi/2$, because of the choice of the f_m^-). To that aim, we use the following relations

$$\left\{ \begin{array}{l} \displaystyle\int_{-\varphi/2}^{\varphi/2} \mathrm{d}y_2 \; Q^-(0,y_2) f_m^-(y_2) = \int_{-\varphi/2}^{\varphi/2} \mathrm{d}y_2 \; Q^+(0,y_2) f_m^-(y_2), \\ \displaystyle\int_{-\varphi/2}^{\varphi/2} \mathrm{d}y_2 \; \frac{\partial Q^-}{\partial y_1}(0,y_2) f_m^{+*}(y_2) = \int_{-1/2}^{1/2} \mathrm{d}y_2 \; \frac{\partial Q^+}{\partial y_1}(0,y_2) f_m^{+*}(y_2), \end{array} \right. \tag{A3}$$

with f_m^{+*} the conjugate of f_m^+ (f_m^- is real). The first relation is the matching of the values in the region $y_2 \in [-\varphi/2, \varphi/2]$ where Q^- is defined. The second relation has more information: we have used that the $\partial_{y_1} Q^+ = 0$ for $|y_2| > \varphi/2$, from which

$$\int_{-1/2}^{1/2} \mathrm{d}y_2 \; \frac{\partial Q^+}{\partial y_1}(0,y_2) f_n^{+*}(y_2) = \int_{-\varphi/2}^{\varphi/2} \mathrm{d}y_2 \; \frac{\partial Q^+}{\partial y_1}(0,y_2) f_m^{+*}(y_2), \tag{A4}$$

afterwards we ask, on average, $\partial_{y_1} Q^+ = \partial_{y_1} Q^-$ for $|y_2| < \varphi/2$. We get a matrix system for the two vectors $\mathbf{q}^- = (q_n^-)_{n=0,\ldots,N^-}$ and $\mathbf{q}^+ = (q_n^+)_{n=0,\ldots,N^+}$ of the form

$$\begin{pmatrix} \mathsf{I} & -{}^t\mathsf{F}^* \\ \mathsf{F}\mathsf{A}\tanh(\mathsf{A}e) & \mathsf{B} \end{pmatrix} \begin{pmatrix} \mathbf{q}^- \\ \mathbf{q}^+ \end{pmatrix} = \begin{pmatrix} \mathbf{S} \\ \mathbf{0} \end{pmatrix}, \tag{A5}$$

with I the $N^- \times N^-$ identity matrix, $\mathsf{A} = \mathrm{diag}(a_n)$, $\mathsf{B} = \mathrm{diag}(|b_n|)$, $F_{mn} = \int_{-\varphi/2}^{\varphi/2} \mathrm{d}y_2 f_n^{+*}(y_2) f_n^-(y_2)$

and $S_n = \int_{-\varphi/2}^{\varphi/2} \mathrm{d}y_2\, y_2 f_n^-(y_2)$. The expressions of F_{mn} and S_n are given below

$$\begin{cases} F_{mn} = \sqrt{\dfrac{\varphi}{2}} \left[\mathrm{sinc}((a_n - b_m)\varphi/2) e^{\mathrm{i}n\pi/2} + \mathrm{sinc}((a_n + b_m)\varphi/2) e^{-\mathrm{i}n\pi/2} \right], \\ S_n = -2\sqrt{\dfrac{2}{\varphi}} \dfrac{1}{a_n^2} \end{cases} \tag{A6}$$

The system is of the form $\mathsf{M}\mathbf{q} = \mathbf{s}$ with the matrix M being square (this is not always the case in systems written using mode matching). Next, M is invertible if one has taken care to consider only the antisymmetric modes. Thus, the system can be solved to find $\mathbf{q}$ by inverting M or it can be solved in the least squares sense (as done by the operation $\mathsf{M}\backslash\mathbf{s}$ in Matlab).

Then, we want to determine

$$\mathcal{C} = -\int \mathrm{d}\mathbf{y}\, \frac{\partial Q^{(2)}}{\partial y_2} = \int_{-e}^{0} \mathrm{d}y_1 \int_{-\varphi/2}^{\varphi/2} \left[1 - \frac{\partial Q^-}{\partial y_2} \right]. \tag{A7}$$

where we have used that $Q^{(2)}(y_1 \geq 0, y_2) = Q^+(\mathbf{y}) - y_2$ is periodic, thus of vanishing contribution. It is now sufficient to write $\mathcal{C} = e\varphi - q_n^- \mathrm{tanh} a_n e / a_n [f_n]_{-\varphi/2}^{\varphi/2}$ to get

$$\mathcal{C} = e\varphi + 2\sqrt{\frac{2}{\varphi}} \frac{\mathrm{tanh} a_n e}{a_n}\, q_n^-. \tag{A8}$$

The procedure of mode matching is longer to explain than to encode; below is a script working with Matlab.

Appendix B: Alternative derivation of the jump conditions

In [18, 19], jump conditions are determined for a zero thickness interface. In fact, instead of anticipating the use of a thin equivalent interface, it is possible to start from the jump conditions established for the zero thickness interface, namely, these are

$$\begin{cases} [\![P]\!]_0 = h\mathcal{B} \overline{\dfrac{\partial P}{\partial X_1}}_{|0}, \\ [\![U_1]\!]_0 = e(\varphi - 1) \overline{\dfrac{\partial U_1}{\partial X_1}}_{|0} + h\mathcal{C} \overline{\dfrac{\partial U_2}{\partial X_2}}_{|0}, \end{cases} \tag{B1}$$

and in the above conditions, the suffix "0" refers to the zero thickness of the interface. To recover the jump condition in Eqs. (27), it is sufficient to remark that

$$P(-e, X_2, t) = P(0^-, X_2, t) - e\frac{\partial P}{\partial X_1}(0^-, X_2, t) + O(e^2) = P(0^-, X_2, t) - e\overline{\frac{\partial P}{\partial X_1}} + O(e^2),$$

```
function C=func(phi,e,Nd,Np)

nd=1:Nd;          np=[-Np:-1,1:Np];
Nd=length(nd);    Np=length(np);
an=nd*pi/phi;     bn=2*np*pi;

    for mm=1:Np,
       for nn=1:Nd,
          a=an(nn); b=bn(mm); n=nd(nn); EX=exp(1i*n*pi/2);
          temp=sinc((a-b)*phi/(2*pi))*EX+sinc((a+b)*phi/(2*pi))/EX;
          F(mm,nn) = sqrt(phi/2)*temp;
       end,
    end

        MM=[eye(Nd) ,-F';
            F*diag(an.*tanh(an*e)), diag(abs(bn))];

        s=sqrt(2/phi)*(((-1).^nd-1)./an.^2).'; S=[s; zeros(Np,1)];
        q=MM\S;qm=q(1:Nd);

        C=phi*e+sqrt(2/phi)*sum( 2.*qm.'.*tanh(an*e)./an );
end
```

same for U_1, and e is small (to be more consistent, the expansion should be done in $\mathbf{x}$-coordinates, thus $O(\varepsilon^2)$ would appear explicitly). It follows that

$$[\![P]\!] = [\![P]\!]_0 + e\overline{\frac{\partial P}{\partial X_1}},$$

same for U_1 and we indeed recover the Eqs. (27). As previously said, this is done in [18] following this procedure. In fact, in this reference, e is let as a free parameter, and this is meant to ensure the positivity of all the effective parameters for e large enough. Our guess is that e being the actual thickness of the interface is the best choice.

---

[1] J.B. Pendry, L. Martin-Moreno and F.J. Garcia-Vidal, "Mimicking surface plasmons with structured surfaces", Science, **305**, 847–848 (2004).

[2] F.J. Garcia-Vidal, L. Martin-Moreno and J.B. Pendry, "Surfaces with holes in them: new plasmonic metamaterials", J. Opt. A: Pure and Appl. Opt., **7**, S97, (2005).

[3] J. Zhu, J. Christensen, J. Jung, L. Martin-Moreno, X. Yin, L. Fok, X. Zhang, and F.J. Garcia-Vidal, "A holey-structured metamaterial for acoustic deep-subwavelength imaging", Nature Physics, **7**, 52–55, 2011.

[4] F. Lemoult, N. Kaina, M. Fink and G. Lerosey, "Wave propagation control at the deep subwavelength scale in metamaterials", Nature Physics, **9**, 55–60, 2013.

[5] G. Ma, M. Yang, S. Xiao, Z. Yang and P. Sheng, "Acoustic metasurface with hybrid resonances", Nature Materials **13**, 873-878 (2014).

[6] J. Zhao, H. Ye, K. Huang, Z.N. Chen, B. Li and C.W. Qiu, "Manipulation of acoustic focusing with an active and configurable planar metasurface transducer", Scient. Rep., **4**, 6257 (2014).

[7] P. Peng, B. Xiao, and Y. Wu, "Flat acoustic lens by acoustic grating with curled slits", Phys. Lett. A, **378**, 3389–3392 (2014).

[8] Y. Li, X. Jiang, R. Li, B. Liang, X. Zou, L. Yin and J. Cheng, "Experimental realization of full control of reflected waves with subwavelength acoustic metasurfaces", Phys. Rev. Appl., **2**, 064002, (2014).

[9] Y. Xie, W. Wang, H. Chen, A. Konneker, B.-I. Popa, and S.A. Cummer, "Wavefront modulation and subwavelength diffractive acoustics with an acoustic metasurface", Nature Com., **5**: 5553 (2014).

[10] J. Zhu, C. Yongyao, X. Zhu, F. Garcia-Vidal, X. Yin, W. Zhang and X. Zhang, "Acoustic rainbow trapping", Scient. Rep., **3**:1728 (2013).

[11] A. Maurel, S. Félix and J.-F. Mercier, "Enhanced transmission through gratings: Structural and geometrical effects", Phys. Rev. B, **88**, 115416 (2013).

[12] C.R. Simovski, "On electromagnetic characterization and homogenization of nanostructured metamaterials", J. Optics, **13**, 013001 (2011).

[13] C.L. Holloway, A. Dienstfrey, E.F. Kuester, J.F. O'Hara, A.K. Azad, and A.J. Taylor, "A discussion on the interpretation and characterization of metafilms/metasurfaces: The two-dimensional equivalent of metamaterials", Metamaterials, **3** 100–112 (2009).

[14] P.A. Martin, R.A. Dalrymple, "Scattering of long waves by cylindrical obstacles and gratings using matched asymptotic expansions", Journal of Fluid Mechanics, **188** 465–490 (1988).

[15] A.S. Bonnet-Bendhia, D. Drissi and N. Gmati, "Simulation of muffler's transmission losses by a homogenized finite element method", J. Comp. Acoust., **12**, 447–474 (2004).

[16] Y. Capdeville and J.-J. Marigo, "Second order homogenization of the elastic wave equation for non-periodic layered media", Geophys. J. Int., **170**, 823–838 (2007).

[17] Y. Capdeville, L. Guillot and J.-J. Marigo, "2-d non-periodic homogenization to upscale elastic media for p–sv waves", Geophys. J. Int., **182**, 903–922 (2010).

[18] B. Delourme, H. Haddar and P. Joly, "Approximate models for wave propagation across thin periodic interfaces", J. Math. Pures Appl., **98**, 28–71 (2012).

[19] J.-J. Marigo and A. Maurel, "An interface model for homogenization of acoustic metafilms", DOI: 10.13140/RG.2.1.3667.7206 (2016).

[20] J.-J. Marigo, C. Pideri, "The effective behavior of elastic bodies containing microcracks or microholes localized on a surface", Int. J. Dam. Mech., **20**, 1151–1177 (2011).

[21] D. Martin, J.-J. Marigo and C. Pideri, "Homogenized interface model describing inhomogeneities located on a surface", *J. Elast.*, **109** 153–187 (2012).

[22] R. Abdelmoula, M. Coutris, J.-J. Marigo, "Comportement asymptotique d'une interphase élastique mince", C. R. Acad. Sc. IIB, **326**, 237–242 (1998).

[23] M. Bonnet, A. Burel, M. Duruflé and P. Joly, "Effective transmission conditions for thin-layer transmission problems in elastodynamics. The case of a planar layer model", Mathematical Modelling and Numerical Analysis, 32 (2015).

[24] A. Căbuz, D. Felbacq and D. Cassagne, "Homogenization of negative-index composite metamaterials: A two-step approach", Phys. Rev. Lett., **98**, 037403 (2007).